ELSEVIER

Journal of Structural Geology 28 (2006) 392–407

JOURNAL OF STRUCTURAL GEOLOGY

www.elsevier.com/locate/jsg

The motion of a non-rigid ellipse in a general 2D deformation

Kieran F. Mulchrone *, Killian Walsh

Department of Applied Mathematics, University College, Cork

Received 13 June 2005; received in revised form 2 December 2005; accepted 10 December 2005
Available online 26 January 2006

Abstract

A solution for the deformation of a non-rigid viscous elliptical inclusion in a matrix of differing viscosity is developed for the case of a general 2D deformation. A Newtonian rheology is assumed and velocities and stresses are equated at the boundary. An important parameter is the viscosity ratio given by the ratio of the external to the internal viscosities. The dynamics of the behaviour of such inclusions is examined for the cases of pure and simple shear and variable viscosity ratio. In general less viscous inclusions tend to accumulate finite strain more rapidly than more rigid inclusions. Large discordancies between the internal finite strain ellipse orientation and the bulk external finite strain ellipse are to be expected. It is also found that the kinematics of deformation inside an inclusion can often be one of super shear (i.e. kinematic vorticity number, W_k, greater than one) even though the external bulk kinematics is one of pure or simple shear ($W_k = 0$ or 1). Objects tend to continuously rotate (the viscosity ratio must be less than 0.5) or asymptotically rotate (i.e. tend to ultimately align parallel to a fixed direction). This solution has many applications, some of which are briefly considered.

Keywords: Viscosity ratio; Non-rigid inclusion; Dynamics; Deformation kinematics

1. Introduction

Many areas of understanding in structural geology have benefited from an interaction between field observation, theoretical and experimental models of rock behaviour. For example, the theory of passive deformation (Ramsay, 1967) applied to elliptical objects has lead to the development of the R_f/ϕ (Dunnet, 1969), centre to centre (Fry, 1979) and nearest neighbour (Mulchrone, 2003) methods of strain analysis. An understanding of the behaviour of rigid elliptical objects has helped identify structures useful for identifying shear sense (Passchier and Trouw, 1996, pp. 116–121). In this paper, a general solution for the behaviour of non-rigid, deformable elliptical objects under a general deformation is developed that encompasses both passive and rigid behaviour and intermediate situations.

Some work has been attempted in this area in the past. Gay (1968) developed a model for a non-rotating elliptical object under pure shear flow by extending the model of Taylor (1932) for a circular object, based in turn on a general theory of Lamb (1932, pp. 594–598). Gay's (1968) extended model must be treated with caution because Lamb's formulation "can be applied to the solution of a number of problems where the boundary-conditions have relation to spherical surfaces" (Lamb, 1932, p. 597). Gay (1968) mixes spherical and elliptical coordinates to obtain a solution, for example at the boundary of the ellipse r (circular coordinates) are equated with ρ (elliptical coordinates) (see also Bilby et al., 1975; Bilby and Kolbuszewski, 1977; Treagus and Treagus, 2001). However, it is clear that the results obtained by Gay (1968) serve as a good first approximation for the case of a non-rotating elliptical object in pure shear. Gay (1968) used approximate methods to examine the case of rotation under pure and simple shear.

Bilby and Kolbuszewski (1977) adapted the method of Eshelby (1957) (i.e. for linear elastic fields around ellipsoidal inclusions) and by using the well-known analogy between elasticity and slow incompressible linear viscous flow and linear elasticity, derived a solution for the behaviour of a deformable ellipse. The approach taken here extends the work of Jefferys (1922) and even though the resulting equations are probably identical to those of Bilby and Kolbuszewski (1977), our approach is original and gives the solution for flow both inside and outside the ellipse during a general deformation explicitly. Due to the long standing interest in Jefferys work in structural geology we believe our solution is in a more comprehensible format and we provide applications of geological interest. Treagus and Treagus (2001) used the work of Bilby et al. (1975) and Bilby and Kolbuszewski (1977)

* Corresponding author. Tel.: +353 21 4903411; fax: +353 21 4271040.
E-mail address: k.mulchrone@ucc.ie (K.F. Mulchrone).

0191-8141/$ - see front matter © 2006 Elsevier Ltd. All rights reserved.
doi:10.1016/j.jsg.2005.12.008

to investigate the influence of object shape on strain in the case of axes parallel or parallel to a pure shearing deformation. Recently Schmid and Podladchikov (2003) derived a solution to the problem considered here by applying Mukhelishvili's method. In deriving estimates for the bulk properties of a dispersion of aligned elliptical inclusions in a host, Fletcher (2004) considers the case of an anisotropic viscous inclusion in an anisotropic viscous host material.

In this paper a guide to the theoretical derivation is presented along with a detailed derivation in the Appendices. Particular examples are studied in detail and some results are presented. After a discussion of potential applications in the areas of strain analysis, fabrics, strain patterns and strain refraction, the paper is concluded.

2. Guide to the solution

The model developed here is based on the solution for a rigid object immersed in a viscous fluid by Jefferys (1922); however, it differs quite significantly in the way velocities and stresses are handled and equated at the boundary. A detailed derivation is presented in the Appendices. The rotational convention adopted here is that the direction along the positive x-axis is 0° and that anti-clockwise is the positive direction. At any time instant the model consists of a non-rigid elliptical object of viscosity μ_i immersed in a matrix of viscosity μ_e whose long axis makes an angle ϕ with the positive x'-direction (see Fig. 1) and whose long and short axes are a and b, respectively. The viscosity ratio is defined as $\mu_r = \mu_e/\mu_i$. The (x',y') coordinate system is fixed whereas the (x,y) coordinate system is always defined with respect to the long and short axes of the elliptical object. In the absence of the elliptical object an homogeneous deformation defined by a given velocity gradient tensor ($\mathbf{L}'$) with respect to (x',y') prevails. In the presence of the elliptical object the homogenous deformation is perturbed near the elliptical object, but at large distances from the object this perturbation disappears. Furthermore, we assume that inside the elliptical object a general homogenous deformation occurs (i.e. no perturbation), which is usually different to the unperturbed external deformation. This guarantees that the elliptical object maintains an elliptical shape at all times.

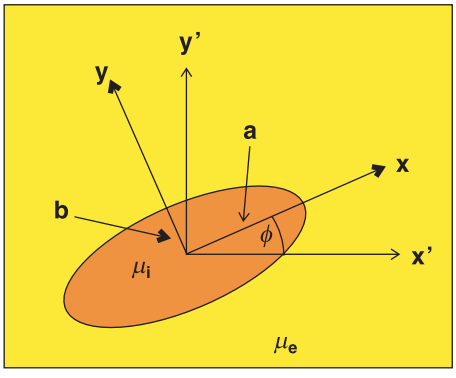

Fig. 1. Setting for the problem. An elliptical inclusion with viscosity μ_i is enclosed in a medium with viscosity μ_e and has long and short semi-axes labelled a and b, respectively. There is a fixed coordinate system (x',y') and a coordinate system that remains parallel to ellipse axes denoted by (x,y).

The derivation proceeds by assuming a form for the perturbed flow velocity field (u,v) in terms of functions that first solve Laplace's equation (i.e. for a function f, $\nabla^2 f = 0$) and second vanishes far from the elliptical object (see Appendices A.3 and A.4). By requiring continuity/equality of velocity at the ellipse boundary the external velocity field can be written in terms of the internal velocity field, the unperturbed flow and the instantaneous shape of the ellipse (see Eq. (61)). Using the solution for the external velocity field and the assumed internal velocity field, both the internal and external stresses can be calculated (see Eqs. (62) and (63)). By requiring equality of stresses at the boundary, the remaining unknown parameters for the internal velocity field can be calculated (see. Eq. (67)). Therefore the internal and perturbed velocity fields are all known and the problem is solved.

3. Results

In this section a number of situations are investigated with the new solution. It is necessary to calculate the finite strain state inside the elliptical object. However, this turns out to be relatively easy because a homogeneous deformation is present inside the object. The method given by Mancktelow (1991) (see also Middleton and Wilcock, 1994, pp. 244–245) is followed. For convenience the points (0,1) and (1,0), which map to the points (x_p,y_p) and (x_q,y_q), respectively, after deformation, are chosen. Then the strain matrix of Ramsay and Huber (1983, p. 283) is given by:

$$\begin{pmatrix} x_q & x_p \\ y_q & y_p \end{pmatrix}$$

and the equations of Ramsay and Huber (1983, pp. 283–287) can be used to calculate the finite strain state. The points (x_p,y_p) and (x_q,y_q) are calculated by numerically solving the system of ordinary differential equations given by Eqs. (68), (73) and (77) subject to appropriate boundary conditions.

3.1. Pure shear deformation of a particle with its axes parallel to the stretching direction

This situation has already been discussed by Bilby et al. (1975), Bilby and Kolbuszewski (1977) and Treagus and Treagus (2001). Under a pure shear deformation $L'_{12} = L'_{21} = 0$ and because the particle axes parallel the stretching directions $\phi = 0$ or $\pi/2$, $\sin\phi = 0$, the ellipse rotation rate is zero (see Eq. (73)). The short and long axes of the particle will change according to Eq. (77) so that the rate of change of the particle aspect ratio $(R = a/b)$ is:

$$\frac{dR}{dt} = \frac{1}{b^2}\left(\frac{da}{dt}b - \frac{db}{dt}a\right) = \frac{2L'_{11}\mu_r R(1+R)^2}{\mu_r(1+R^2)+2R} \quad (1)$$

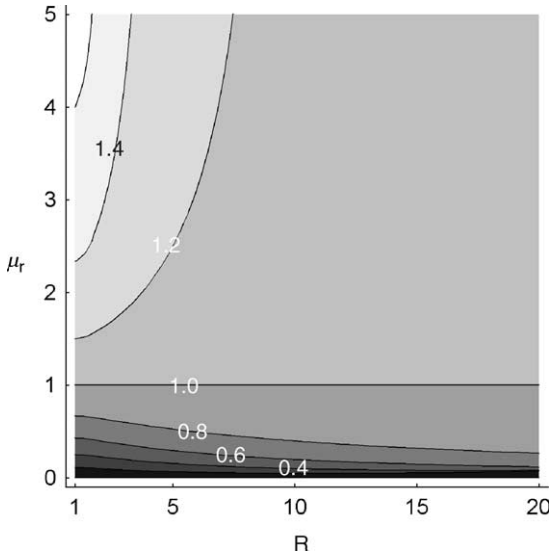

Fig. 2. Contours of the rate of deformation of an ellipse relative to a similarly shaped passive object whose long axes parallel the stretching axis in pure shear.

For a passively deforming particle $\mu_r = 1$ in the same situation:

$$\frac{dR}{dt} = 2L'_{11}R \tag{2}$$

By finding the ratio of Eqs. (1) and (2), the rate of change of a particle can be compared with that of a passive particle as:

$$\frac{\mu_r(1+R)^2}{\mu_r(1+R^2)+2R} \tag{3}$$

As illustrated in Fig. 2 as the particle becomes progressively more rigid (i.e. $\mu_r < 1$) it deforms more slowly than the surrounding material and vice versa for less rigid particles ($\mu_r > 1$). This comparison is only valid for two objects that instantaneously have the same axial ratio (R). However, in the limit as $R \to \infty$ (i.e. the particle becomes a layer) the ratio becomes unity so that a layer deforms in the same way as its surrounding material independent of μ_r. This is in agreement with the analyses of Smith (1975), Fletcher (1977) and Johnson and Fletcher (1994, pp. 46–47) for the mean flow of a layer enclosed in a material of a different viscosity. However, from the analysis of Gay (1968) as $R \to \infty$ this ratio is:

$$\frac{5\mu_r}{2+3\mu_r} \tag{4}$$

implying that layers deform at different rates to the surrounding material except in the case that the internal and external viscosities are equal, in contradiction of other theories. For $\mu_r = 0$ there is no shape change corresponding to a rigid particle and as $\mu_r \to \infty$ (corresponding to an area-preserving void) an upper limit for the rate of shape change emerges:

$$\frac{(1+R)^2}{(1+R^2)} \tag{5}$$

3.2. Pure shear deformation of a particle with its axes oblique to the stretching direction

Any deviation from the simple premises of the previous section involves solving the full set of equations (Eqs. (68), (73) and (77)). However, in the case of pure shear ($L'_{12} = L'_{21} = 0$) from which the motion of an non-rigid ellipse is given by:

$$\begin{aligned}\frac{d\phi}{dt} &= \frac{L'_{11}(R+1)(1+2R(\mu_r-1)+R^2)\sin(2\phi)}{(R-1)(1+2\mu_r R+R^2)}\\ \frac{dR}{dt} &= \frac{2L'_{11}\mu_r\cos(2\phi)R(1+R)^2}{\mu_r(1+R^2)+2R}\end{aligned} \tag{6}$$

In the case of a passive elliptical object the equations governing its motion are found by setting $\mu_r = 1$:

$$\frac{d\phi}{dt} = \frac{L'_{11}(R^2+1)\sin(2\phi)}{(R^2-1)} \qquad \frac{dR}{dt} = 2L'_{11}\cos(2\phi)R$$

therefore, the rates of change relative to that of a passive marker (for orientation and axial ratio respectively) are:

$$\frac{(R+1)^2(1+2R(\mu_r-1)+R^2)}{(R^2+1)(1+2\mu_r R+R^2)} \qquad \frac{\mu_r(1+R)^2}{\mu_r(1+R^2)+2R} \tag{7}$$

It is important to note that these comparisons are valid only for objects instantaneously sharing the same orientation and axial ratio. First of all it is clear that the rate of change of axial ratio is the same as that for an ellipse parallel to the stretching axis by comparing Eqs. (3) and (7) and Fig. 2 displays its characteristics. Fig. 3 illustrates the situation for rate of rotation. Elliptical objects that are less viscous than the surrounding medium rotate faster than passive markers, whereas those that are more viscous rotate more slowly. However, this effect lessens as the axial ratio increases.

In the oblique case, the evolution of a non-rigid object will be more complex as the rate of change of the axial ratio depends on orientation as well as the current axial ratio. In Fig. 4a an example is shown that illustrates rapid accentuation of axial ratio of a less

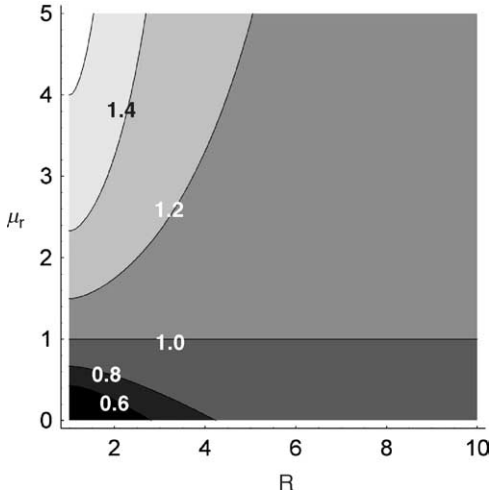

Fig. 3. Contours of the rate of rotation of an ellipse relative to that of a similarly shaped passive object under pure shear.

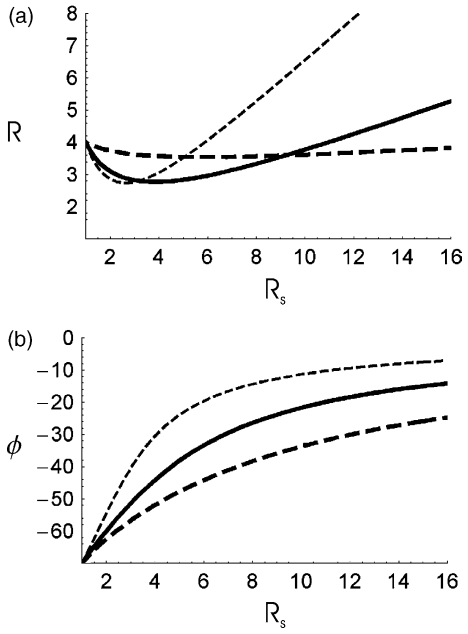

Fig. 4. Elliptical object oriented obliquely to the stretching axis (initially at −70°) with an initial axial ratio of 4. Solid line illustrates passive marker behaviour ($\mu_r = 1.0$), thick dashed line represents more viscous behaviour ($\mu_r = 0.1$) and thin dashed line is for less viscous behaviour ($\mu_r = 10$). (a) Variation of object axial ratio versus bulk (i.e. external) finite strain (R_s, the ratio of the long and short axes of the finite strain ellipse). (b) Variation of object orientations versus bulk finite strain.

viscous object, whereas a more viscous object changes its shape less readily by comparison with a passive object. Rotation rates are dramatically affected, as shown in the example in Fig. 4b where less viscous objects rotate much faster than passive objects and more rigid objects tend to rotate more slowly.

In the example in Fig. 4 the bulk strain (or far-field finite strain) increases due to pure shear with stretching axis oriented parallel to the 0°-direction. Likewise the internal strain of a passive marker will match the external strain field exactly. But what about the internal strain history for less or more viscous objects? Fig. 5a and b shows the results for a less viscous object. Remarkably, the object rapidly accumulates finite strain internally and there is an immediate asymmetry between the internal and external finite strain long axis orientations. However, at higher strains the orientation of the internal finite strain ellipse approaches that of the external finite strain ellipse and the orientation of the object itself. A more viscous object with the same initial conditions (see Fig. 5c and d) behaves such that the shape of the object becomes elongate without much accumulation of internal finite strain; however, as the object comes into parallelism with the external stretching axis, internal finite strain begins to accumulate quickly. There is a striking difference between the orientation of the strain ellipse and the object orientation that is maintained until high external finite strains have been achieved. This implies that, in general, fabric asymmetries cannot be used alone as reliable kinematic indicators for the bulk external deformation (see for example Passchier and Trouw, 1996, p. 178).

The kinematics of the internal deformation is also of great interest as the external kinematics are pure shear and this solution

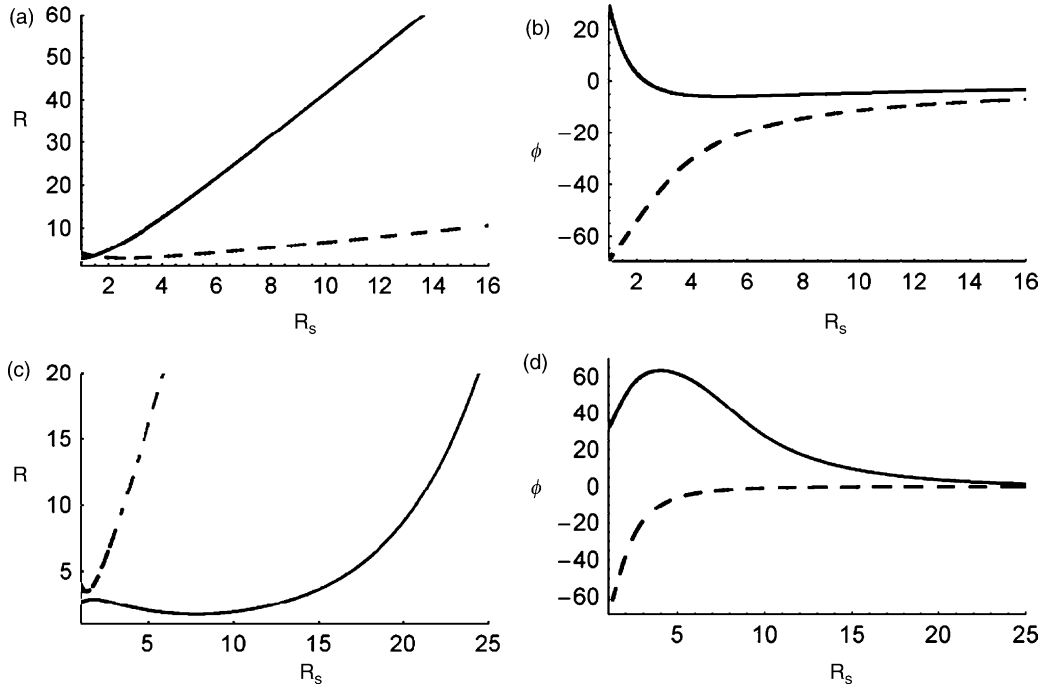

Fig. 5. Internal strain characteristics for a less ($\mu_r = 10$) and more viscous object ($\mu_r = 0.1$) initially oriented at −70° to the pure shear stretching axis with an initial axial ratio of 4. (a) Less viscous. Solid line illustrates the finite strain axial ratio internal to the object, whereas the dashed line illustrates the axial ratio of the object itself. Note that the ordinate axis is graduated according to the external finite strain axial ratio. (b) Less viscous. Solid line illustrates orientation of the internal finite strain ellipse and the dashed line illustrates the orientation of the object itself. (c) More viscous. Solid line illustrates the finite strain axial ratio internal to the object, whereas the dashed line illustrates the axial ratio of the object itself. (d) More viscous. Solid line illustrates orientation of the internal finite strain ellipse and the dashed line illustrates the orientation of the object itself.

allows exploration of how one kinematic state may be contained within another. The kinematic vorticity number (W_k) is used to quantify the kinematics and applying the definition of Ghosh (1987) we find that for an internal deformation it is given by:

$$W_k = \frac{\omega_1 + \omega_2}{\sqrt{4k^2 + (\omega_1 - \omega_2)^2}} \tag{8}$$

where ω_1, ω_2 and k are the components of the velocity gradient tensor of the internal deformation (see the Appendices). Upon substitution of Eq. (67) and the flow field with respect to the fixed axes we have:

$$W_k = \frac{(L'_{12} - L'_{21})(1 + 2\mu_r R + R^2) + (\mu_r - 1)(R^2 - 1)\left[(L'_{12} + L'_{21})\cos(2\phi) - 2L'_{11}\sin(2\phi)\right]}{(1 + 2\mu_r R + R^2)\sqrt{\mu_r^2(1+R)^4\left[\frac{\left((L'_{12}+L'_{21})\cos(2\phi) - 2L'_{11}\sin(2\phi)\right)^2}{(1+2\mu_r R+R^2)^2} + \frac{\left(2L'_{11}\cos(2\phi) + (L'_{12}+L'_{21})\sin(2\phi)\right)^2}{(\mu_r + 2R + \mu_r R^2)^2}\right]}} \tag{9}$$

and in the case of pure shear this reduces to:

$$W_k = \frac{L'_{11}\sin(2\phi)(\mu_r - 1)(R^2 - 1)}{(1 + 2\mu_r R + R^2)\sqrt{L'^2_{11}\mu_r^2(1+R)^4\left[\frac{\sin^2(2\phi)}{(1+2\mu_r R+R^2)^2} + \frac{\cos^2(2\phi)}{(\mu_r + 2R + \mu_r R^2)^2}\right]}} \tag{10}$$

Note that the absolute value of L'_{11} cancels out this expression, although its sign is important. Fig. 6 illustrates W_k for a range of ellipse R and ϕ values. In Fig. 6a a less-viscous elliptical inclusion is present ($\mu_r = 10$) and it is found that an obliquely oriented object internally undergoes intermediate shear (i.e. between pure and simple shear) in a sense opposite to the sense of rotation of the object itself. For example a dextrally rotating object undergoes sinistral shear. If the limit as $R \to \infty$ for Eq. (10) is taken, then the situation for an infinitely long layer (or very long elliptical object) can be assessed. The resulting expression is:

$$W_k = \frac{L'_{11}\sin(2\phi)(\mu_r - 1)}{\sqrt{L'^2_{11}\left(\mu_r^2\sin^2(2\phi) + \cos^2(2\phi)\right)}} \tag{11}$$

From Fig. 7a it is clear that as the enclosed layer becomes less competent simple shear dominates provided the layer is somewhat obliquely oriented. Notice that as passive behaviour is approached (i.e. $\mu_r = 1$) the behaviour inside the layer is the same as that outside, i.e. $W_k = 0$.

A different behaviour emerges in the case of a more viscous object. In Fig. 6b the situation for $\mu_r = 0.1$ is presented. Close to the stretching and shortening direction and for low R, intermediate shear occurs, with a sense of shear synthetic to the object rotation sense, e.g. for $\phi > 0$, the object rotates dextrally and internal dextral shearing occurs. Significantly, for $10° < (\phi (< 80°$ and $R > 1.5$ (approximately) super shear occurs (i.e. a pulsating strain history; Ramberg, 1975), again with a sense of shear consistent with the object rotation sense. Note that elliptical objects tend to rotate into parallelism with the stretching direction implying that in the present case super shear will be temporary. However, it does raise the prospect that super shear may be much more common than previously supposed in natural rocks consisting of inclusions and/or inside larger scale inclusions. In the case of infinitely long more viscous layers a wide range of behaviours exist (see Fig. 7b). Super shear only occurs for $\mu_r < 0.5$ and a restricted range of angles and in all other cases intermediate shear occurs.

3.3. Bulk simple shear deformation

In this section the behaviour of competent and incompetent elliptical inclusions are investigated under a bulk simple shear strain regime. This situation was considered by Bilby and Kolbuszewski (1977), but they did not look at the internal finite strain history. Taking $L'_{11} = L'_{22} = L'_{21} = 0$ the equations governing the motion are given by:

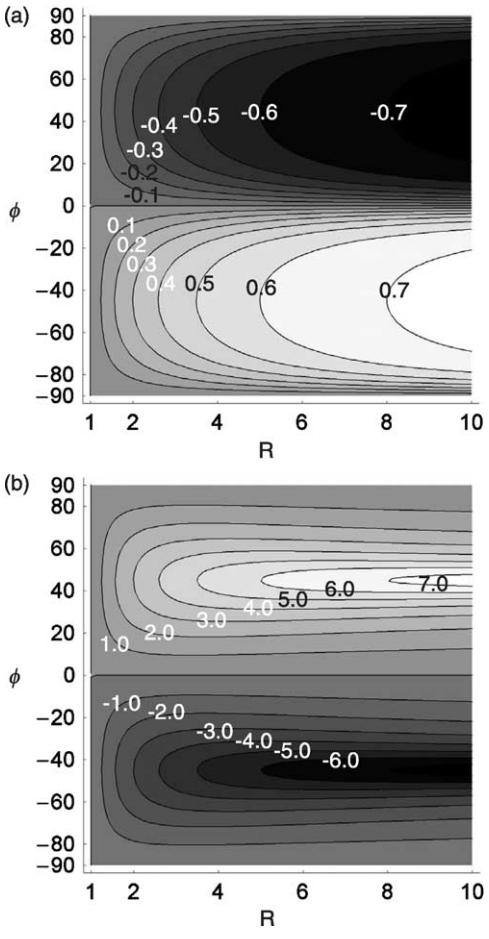

Fig. 6. Internal deformation characteristics of both a more and less viscous inclusion in a pure shear deformation. Contours are for kinematic vorticity (W_k). (a) Less viscous elliptical inclusion ($\mu_r = 10$). (b) More viscous elliptical object ($\mu_r = 0.1$).

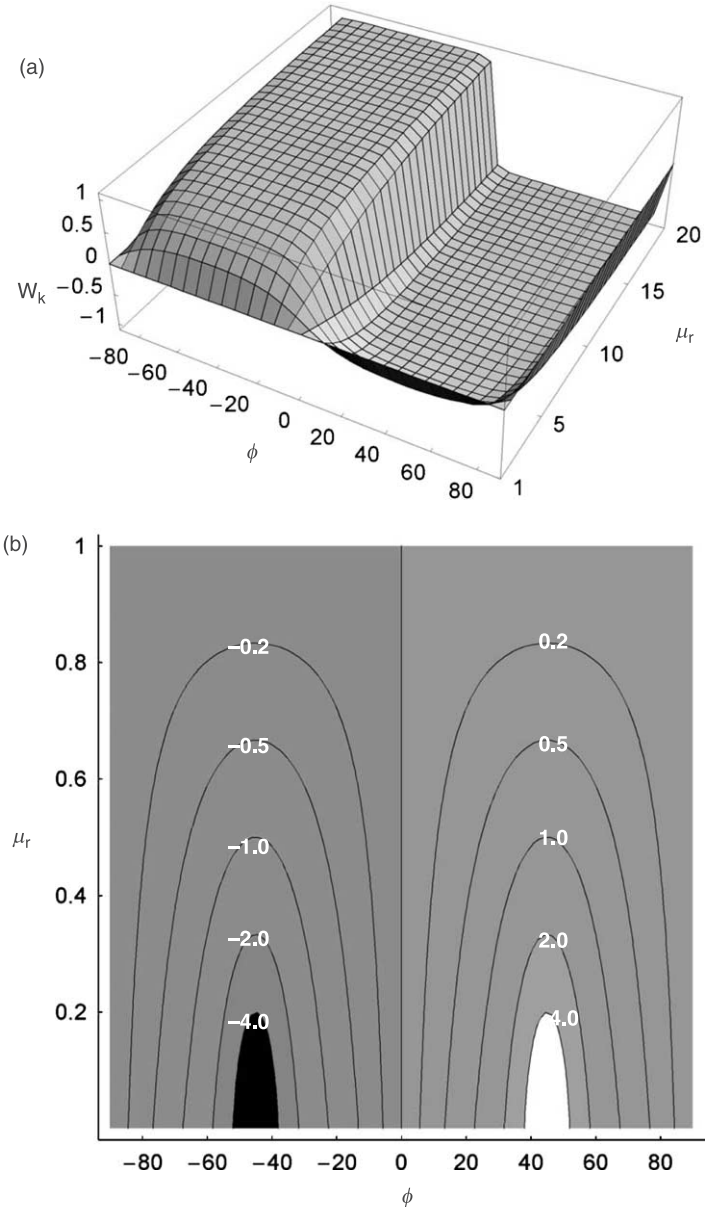

Fig. 7. Behaviour of very long (layer-like) inclusions. (a) 3D plot of W_k versus ϕ and μ_r. In this case the object is less viscous i.e. $\mu_r > 1$. (b) Contour plot for more viscous objects ($0 < \mu_r < 1$).

$$\frac{d\phi}{dt} = \frac{L'_{12}\left[(R(2\mu_r - 1) + 1)\cos^2\phi - R^2(R + 2\mu_r - 1)\sin^2\phi\right]}{(R-1)(R^2 + 2\mu_r R + 1)}$$

$$\frac{dR}{dt} = \frac{2L'_{12}\mu_r R(R+1)^2\sin(2\phi)}{2\mu_r(R^2+1) + 2R} \tag{12}$$

and by letting $\mu_r = 1$ the corresponding passive behaviour is described by:

$$\frac{d\phi}{dt} = \frac{L'_{12}(\cos^2\phi - R^2\sin^2\phi)}{R^2 - 1} \qquad \frac{dR}{dt} = L'_{12}R\sin(2\phi) \tag{13}$$

so that the rates of change relative to a passive marker are given by:

$$\frac{\cos(2\phi)(R+1)^2(R^2 + 2(\mu_r - 1)R + 1) - (R^2-1)(R^2 + 2\mu_r R + 1)}{2(R^2 + 2\mu_r R + 1)(\cos^2\phi - R^2\sin^2\phi)}$$

$$\frac{\mu_r(1+R)^2}{\mu_r(1+R^2) + 2R}$$

Clearly the relative rate of change of R is the same as that for an object under pure shear (see Fig. 2). However, the situation for relative rotation rates is much more complex and additionally depends on orientation. In this case it is easier to directly consider the expressions given in Eq. (12).

An important feature of the solution is exhibited by Eq. (12), also a feature of the general case (Eq. (73)). When the object becomes circular (i.e. $a \to b$ or $R \to 1$) the expression for rate of rotation (of the long axes as opposed to material rotation)

becomes infinite. This is a mathematical artefact arising because the derivation hinges on attaching a coordinate system to an elliptical object. However, in the absence of a long axis (i.e. a circle) this approach fails. It is interesting to note that in the case of a perfectly rigid object ($\mu_r=0$) the expression for rotation rate becomes:

$$\frac{d\phi}{dt}=\frac{-L'_{12}[\cos^2\phi+R^2\sin^2\phi]}{(R^2-1)}$$

due to $(R-1)$ cancelling out above and below the line (see also Eq. (48)). Therefore, in the special case of a rigid object this artefact disappears.

In order to understand the behaviour of objects a little analysis is required. Fixed points are first determined by setting the differential equations in Eq. (12) to zero (i.e. these are points where the rates of change are zero) and solving for both R and ϕ. There is only one solution given by:

$$R* =\frac{1}{1-2\mu_r},\quad \phi* =0 \tag{14}$$

and from the constraints that $R\geq 1$ and the expression beneath the line for R^* must not be zero, we find that this fixed point can only exist for $0\leq\mu_r<0.5$. This indicates fundamentally different kinds of dynamical behaviour for $\mu_r<0.5$ and $\mu_r\geq 0.5$. In the rigid case ($\mu_r=0$) the fixed point only exists for $R^*=1$, i.e. a circular object. Using the terminology of Mulchrone et al. (2005), the dynamics of the behaviour of non-rigid objects consists of continuous and asymptotic rotations. It can be shown using the techniques of non-linear dynamics (see for example Strogatz, 1994; Chang Man Fong and De Kee, 1999, p. 17) that the fixed point is at the centre of closed periodic trajectories. Therefore for $\mu_r<0.5$ we expect objects to continuously rotate as R periodically rises and falls (see Fig. 8a). It is also noted that for $\phi=\pm\pi/2$, $dR/dt=0$. It is also interesting to note that at the fixed point the solution is one where neither the shape nor orientation of the ellipse changes during simple shear, a behaviour previously reported by Bilby and Kolbuszewski (1977).

By considering the expression for rotation rate (in Eq. (12)), equating it with zero and solving it for ϕ, curves that objects tend to rotate away from or towards are derived:

$$\phi=\pm\cos^{-1}\left(R\sqrt{\frac{R+2\mu_r-1}{(R+1)(R2+2(\mu_r-1)+1)}}\right) \tag{15}$$

By looking at the rate of change of rotation rate it is found that objects rotate towards the positive curve and away from the negative curve (see also Fig. 8). For $\mu_r<0.5$ the positive and negative curves coalesce to form a closed curve (see Fig. 8a). Inside this curve objects continuously rotate without turning a full circle. An example solution is shown in Fig. 9. Objects attain their maximum R at $\phi=0$ and the orientation flips instantaneously when $R=1$. This is a newly discovered behaviour. Outside the curve, objects rotate through a full circle similar to the already known trajectories of rigid objects

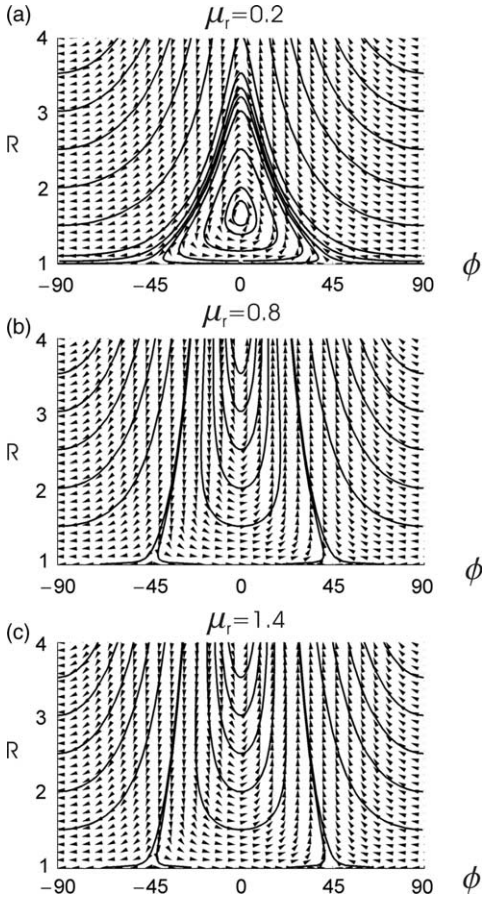

Fig. 8. Phase diagrams for the solutions of Eq. (12). For a given value of (R,ϕ), the path taken (i.e. how R and ϕ change over time) can be judged by following the arrows. Solid lines are example paths. Note closed loops in centre of (a), which surround the single fixed point occurring for $\mu_r<0.5$. Note also in (b) and (c) that lines tend to converge on lines emanating from close to $\pm 45°$; these curves correspond to Eq. (15).

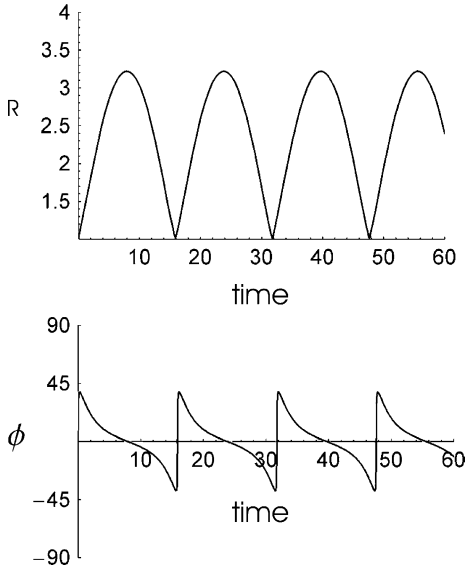

Fig. 9. Example solution for $\mu_r=0.2$. Note the periodic oscillation of both R and ϕ. The maximum value of R corresponds to the position where the object is parallel to the shear plane.

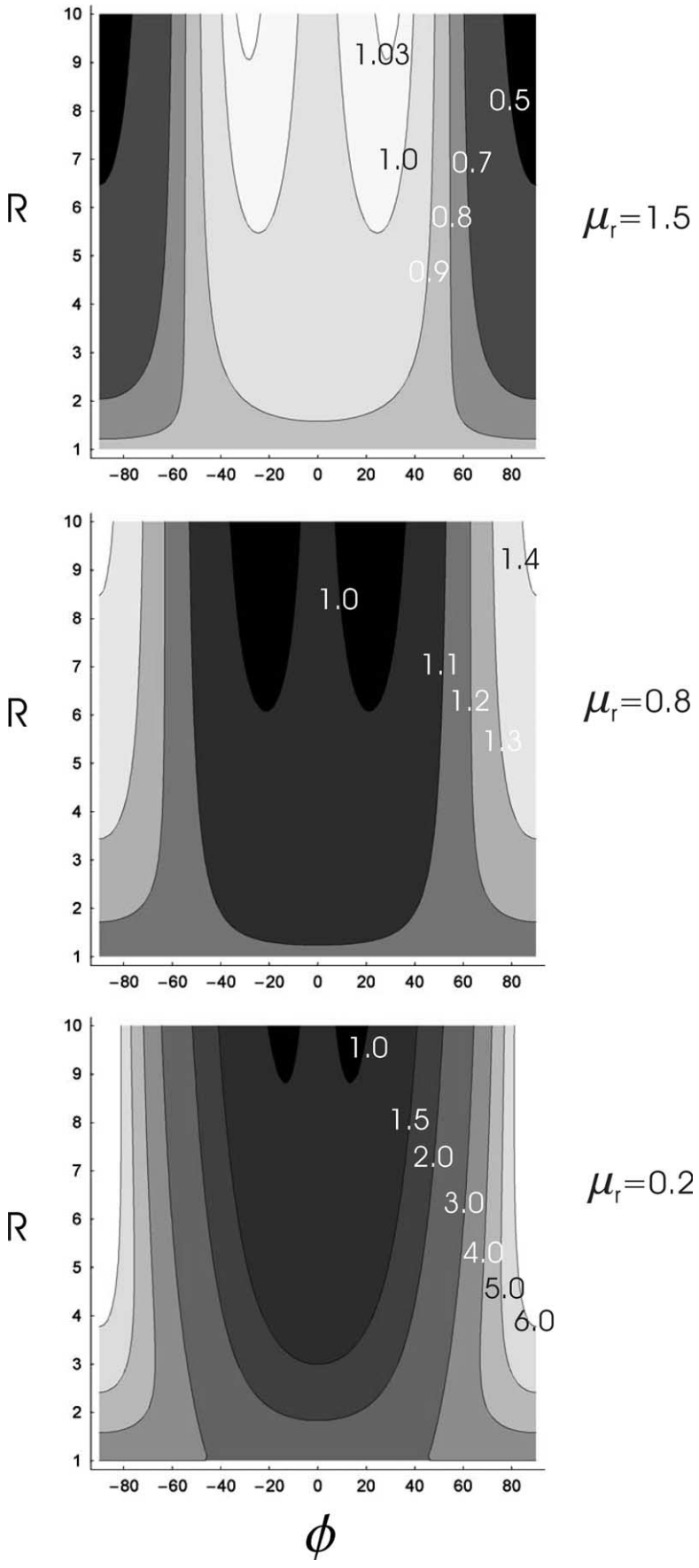

Fig. 10. Internal deformation characteristics of both a more and less viscous inclusion in a simple shear deformation. Contours are for kinematic vorticity (W_k).

(Ghosh and Ramberg, 1976) but clearly the details are different.

By contrast for $\mu_r \geq 0.5$, a different regime is encountered in the absence of a fixed point (see Fig. 8b and c). In this case objects are ultimately aligned parallel to the shear direction. Objects rotate towards the positive curve in Eq. (15) and away from the negative curve. This behaviour is similar to that exhibited by passive objects; however, the details will differ greatly.

Modification of Eq. (9) for the case of simple shear leads to an expression for the kinematics of deformation inside the object as follows:

$$W_k = \frac{L'_{12}[1+2\mu_r R+R^2+\cos(2\phi)(\mu_r-1)(R^2-1)]}{(1+2\mu_r R+R^2)\sqrt{L'^2_{12}\mu_r^2(1+R)^4\left[\frac{\sin^2(2\phi)}{(\mu_r+2R+\mu_r R^2)^2}+\frac{\cos^2(2\phi)}{(1+2\mu_r R+\mu_r R^2)^2}\right]}}$$

Contour plots for W_k are presented in Fig. 10 for $\mu_r = 1.5$, 0.8 and 0.2. Less viscous objects internally undergo intermediate shear, whereas more viscous objects tend to undergo super-shear ($W_k > 1$) for the most part. This becomes accentuated for very rigid objects culminating of course for totally rigid objects undergoing a rigid rotation corresponding to $W_k = \infty$. It is no surprise then that the internal finite strain histories for $\mu_r < 1$ tend to be dominated by pulsating histories, as demonstrated to occur for $W_k > 1$ by Ramberg (1975).

Fig. 11 shows the evolution of the shape and orientation of passive, more and less viscous objects under simple shear by comparison with the accumulated bulk (i.e. external) finite strain. Clearly the shape of the less viscous object rapidly attains a high aspect ratio by comparison with the passive object, whereas the shape of the more viscous object changes much more slowly. After very high strains the more rigid object has the potential to obtain a lower aspect ratio (see the example in Fig. 9). Object orientations are broadly similar but initially, at least, the less viscous object rotates faster than the passive object and the more rigid object rotates the slowest. Eventually both the passive and less viscous objects will line up with the shear plane, whereas the more rigid object has the capacity to rotate right around (in this particular instance it would take very high strains before this occurs).

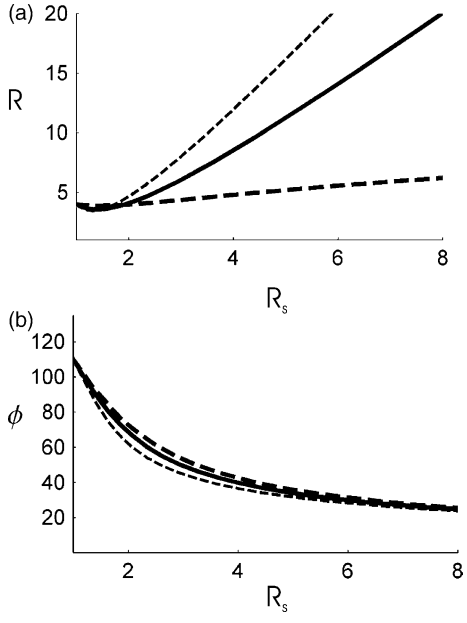

Fig. 11. Elliptical object oriented obliquely to the shear plane (initially at 110°) with an initial axial ratio of 4. Solid line illustrates passive marker behaviour ($\mu_r = 1.0$), thick dashed line represents more viscous behaviour ($\mu_r = 0.1$) and thin dashed line is for less viscous behaviour ($\mu_r = 10$). (a) Variation of object axial ratio versus bulk (i.e. external) finite strain (R_s). (b) Variation of object orientations versus bulk finite strain.

Under bulk simple shear the internal characteristics of strain in a less viscous object (see Fig. 12a and b) demonstrates more rapid accumulation of internal finite strain by comparison with the object aspect ratio. Also, large differences between the internal finite strain ellipse orientation and the object orientation are to be expected and can persist to very high levels of external finite strain. In the case of a more rigid object (see Fig. 12c and d), the object aspect ratio tends to increase whilst the internal finite strain axial ratio decreases, due to the dominance of super shear internally (see Fig. 10c). Additionally, large differences between the finite strain ellipse orientation and object orientation are expected and whilst the object orientation tends to parallel the shear plane (at the scale illustrated) the finite strain ellipse orientation crosses the shear plane, but ultimately tend to parallel the shear plane.

Considering the situation where $\mu_r < 0.5$ and curve objects continuously rotate without turning a full circle (see above), extremely complex finite strain behaviour can occur. Fig. 13 illustrates the situation for $\mu_r = 0.1$ and an initial axial ratio of 1.1 oriented at 110°. The axial ratio of the object periodically rises and falls, whereas the finite strain axial ratio exhibits a periodic oscillation on two scales (see Fig. 13a). Both the object and finite strain orientations fully rotate, although the period of the rotations are out of phase. By comparing Fig. 13a and b it is clear that the large scale oscillation of the finite strain axis coincides with the rotations going in and out of phase.

4. Discussion and applications

The solution presented and investigated in this paper provides a solution for the behaviour of isolated elliptical objects assuming that they undergo homogeneous deformation internally. The solution is flexible in that it encompasses all types of competency contrast and general deformations. The solution should be useful in many geological situations, a few of which will be briefly discussed here.

Methods for strain analysis (see for example Lisle, 1994; Mulchrone et al., 2003) commonly assume passive behaviour of markers, although there are methods which do not (Arbaret et al., 2000; Jezek and Hrouda, 2002a,b; Treagus, 2002; Treagus and Treagus, 2002). There are situations where this assumption does not hold; however, the solution presented here (and its 3D equivalent) will allow this assumption to be relaxed. This will involve future development of new methods for the behaviour of populations of objects under bulk homogeneous deformations. In moving away from passive behaviour, account must be taken of the potential interactions between neighbouring objects. This is also work to be completed in the future.

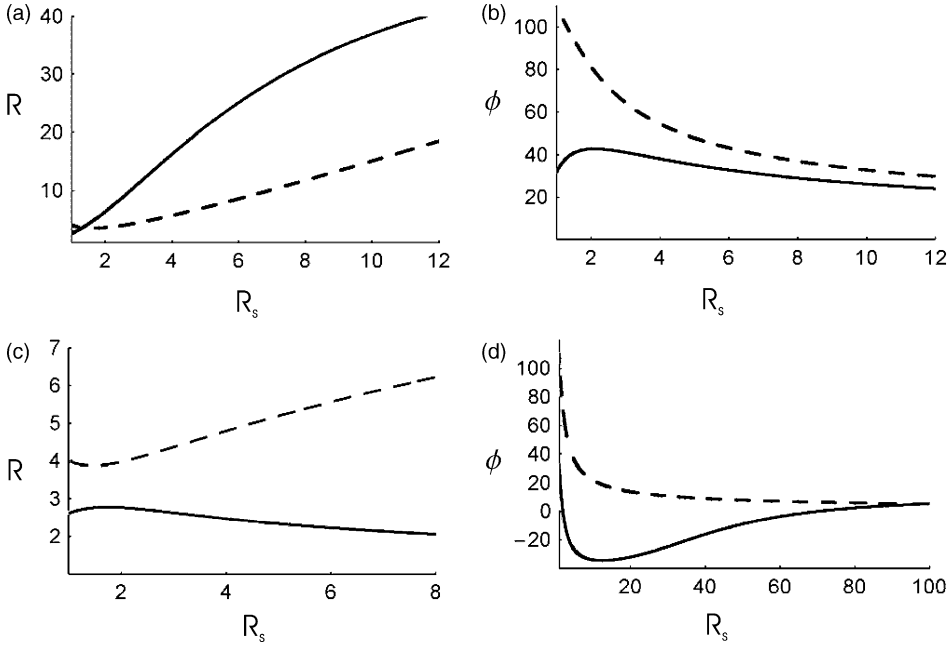

Fig. 12. Internal strain characteristics for a less ($\mu_r = 10$) and more viscous object ($\mu_r = 0.1$) initially oriented at 110° to the shear plane with an initial axial ratio of 4. (a) Less viscous. Solid line illustrates the finite strain axial ratio internal to the object, whereas the dashed line illustrates the axial ratio of the object itself. Note that the ordinate axis is graduated according to the external finite strain axial ratio. (b) Less viscous. Solid line illustrates orientation of the internal finite strain ellipse and the dashed line illustrates the orientation of the object itself. (c) More viscous. Solid line illustrates the finite strain axial ratio internal to the object, whereas the dashed line illustrates the axial ratio of the object itself. (d) More viscous. Solid line illustrates orientation of the internal finite strain ellipse and the dashed line illustrates the orientation of the object itself.

There has been considerable interest recently in the dynamics of flanking structures (Passchier, 2001; Weismayr and Grasemann, 2004). This has involved finite-element modelling (Grasemann and Stüwe, 2001; Grasemann et al., 2003), analogue modelling (Exner et al., 2004) and geometric descriptive schemes (Coelho et al., 2005). The solution developed in this paper is immediately applicable to this situation whereby the CE (i.e. cross-cutting element; Passchier, 2001) is modelled as an elliptical inclusion with high axial ratio

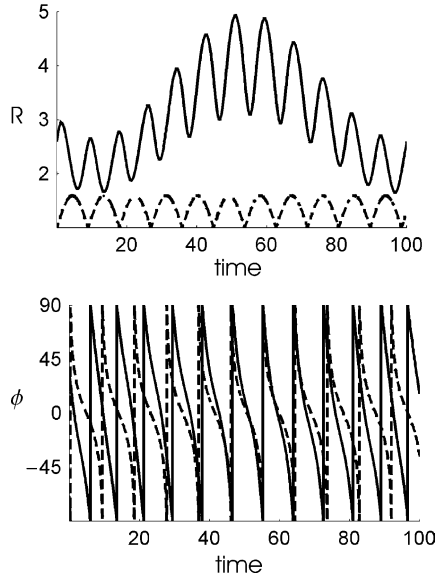

Fig. 13. Internal strain situation for a more rigid object ($\mu_r = 0.1$) initially oriented at 110° to the shear plane with an initial axial ratio of 1.1. (a) Solid line illustrates the finite strain axial ratio internal to the object, whereas the dashed line illustrates the axial ratio of the object itself. Note that the ordinate axis is graduated according to time (at time = 100, the corresponding external finite strain is approximately 10000). (b) Solid line illustrates orientation of the internal finite strain ellipse and the dashed line illustrates the orientation of the object itself.

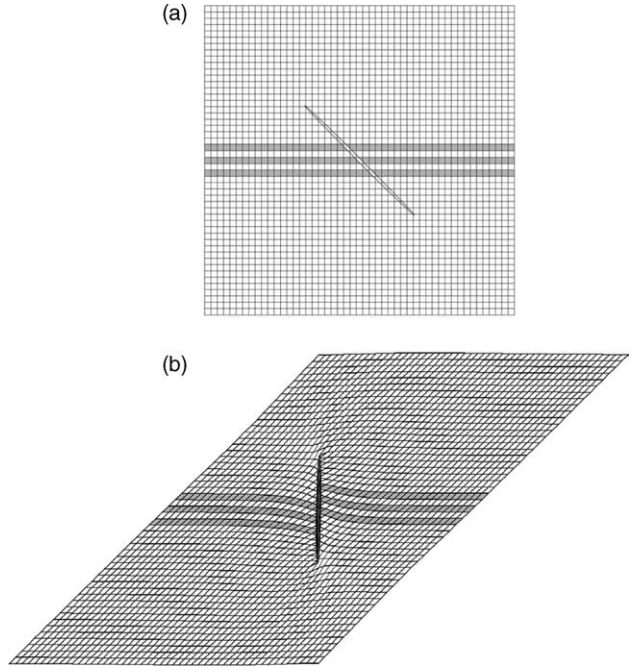

Fig. 14. Application of the developed solution to the modeling of flanking structures. (a) Pre-deformation situation (b) Situation after moderate dextral simple shear.

that can be either more or less viscous than the surrounding medium (the host element, HE). For example in Fig. 14 an elliptical inclusion with an initial axial ratio of 50 is deformed under dextral simple shear with $\mu_r=40$. This example was generated by calculating the positions of grid points using Eqs. (58) and (59) for points outside the ellipse and Eq. (68) for points inside the ellipse and keeping track of which point is connected to which (implemented in Mathematica). From this example alone, some salient features of flanking structures can be discerned. There is a sinistral offset across the CE (antithetic to the bulk dextral shear sense) whilst the gentle flanking folds indicate a dextral shear sense (see for example Exner et al., 2004).

It should also be possible to apply the model in the study of the relationship between internal and external fabrics and their patterns around large scale bodies such as igneous intrusions; however, this has not as yet been attempted. It may also be possible to apply the model to the geometry of shear zones, by modelling shear zones as less viscous elongate inclusions. Furthermore, by studying the relationships between internal and external fabrics a more complete understanding of strain refraction may be achieved.

In conclusion, a solution has been presented for the deformation of viscous elliptical objects immersed in a more or less viscous medium. It is found that complex internal deformation patterns and strain histories can occur even during pure shear deformation. In particular semi-rigid objects during simple shear tend to undergo super-shear deformation. The solution has many potential applications in structural geology.

Acknowledgements

We would like to thank Prof. Ray Fletcher and Dr Joeseph Jezek for their careful, critical and thorough reviews that helped to improve the final manuscript. In particular, Prof. Fletcher pointed out to us the existence of the work by Bilby and Kolbuszewski (1977), which we had failed to identify. Thanks also to Prof. Tom Blenkinsop for editorial assistance. This work was supported in part by the Science Foundation Ireland research frontiers programme (grant 04/BR/ES0020).

Appendix A

In this appendix a detailed derivation of the solution is presented, which is based upon and extends the solution given by Jefferys (1922). Typographical errors in Jefferys (1922) are corrected and an approach consistent with modern structural geology is taken. Hopefully this will enable greater understanding of the approach. We highlight below where our solution departs from that of Jefferys (1922). Essentially the derivation up until Eq. (55) is a 2D analogy of Jefferys (1922) 3D analysis for a rigid object.

A.1. Undisturbed flow

Consider the situation in Fig. 1. If the ellipse was not present, the fluid is assumed to exhibit a homogeneous flow-type given by the velocity gradient tensor $\mathbf{L}'$ so that the velocities u' and v' are:

$$u' = L'_{11}x' + L'_{12}y' \qquad v' = L'_{21}x' + L'_{22}y' \tag{16}$$

however this flow relative to the (x,y) coordinate system is given by:

$$\mathbf{L} = \mathbf{R}L'\mathbf{R}^{\mathrm{T}} \tag{17}$$

where $\mathbf{R}$ is the rotation matrix and superscript T means transpose:

$$\mathbf{R} = \begin{pmatrix} \cos\phi & \sin\phi \\ -\sin\phi & \cos\phi \end{pmatrix} \tag{18}$$

and noting that $L'_{ii}=0$ for isochoric flow:

$$\begin{aligned}
L_{11} &= \frac{1}{2}\left[\left(L'_{11}-L'_{22}\right)\cos(2\phi)+\left(L'_{12}+L'_{21}\right)\sin(2\phi)\right]\\
L_{12} &= \frac{1}{2}\left[L'_{12}-L'_{21}+\left(L'_{12}+L'_{21}\right)\cos(2\phi)+\left(L'_{22}+L'_{11}\right)\sin(2\phi)\right]\\
L_{21} &= \frac{1}{2}\left[L'_{21}-L'_{12}+\left(L'_{12}+L'_{21}\right)\cos(2\phi)+\left(L'_{22}+L'_{11}\right)\sin(2\phi)\right]\\
L_{22} &= \frac{1}{2}\left[\left(L'_{22}-L'_{11}\right)\cos(2\phi)-\left(L'_{12}+L'_{21}\right)\sin(2\phi)\right]
\end{aligned} \tag{19}$$

so that $L_{ii}=0$ as well. Hence the velocity of the unperturbed flow relative to the (x,y) coordinate system is given by:

$$u_0 = L_{11}x + L_{12}y \tag{20}$$

$$v_0 = L_{21}x + L_{22}y \tag{21}$$

A.2. Basic fluid mechanics

From basic fluid mechanics our solution must satisfy some equations (see Johnson and Fletcher (1994, pp. 401–403) or Lai et al. (1993 pp. 355–357) for example):

$$\mu\nabla^2 u = \frac{\partial p}{\partial x} \tag{22}$$

$$\mu\nabla^2 v = \frac{\partial p}{\partial y} \tag{23}$$

$$\frac{\partial u}{\partial x} + \frac{\partial v}{\partial y} = 0 \tag{24}$$

μ is viscosity and p is pressure. For a Newtonian material the stresses are given by:

$$\sigma_{ij} = 2\mu D_{ij} - p\delta_{ij}$$

where $D_{ij} = \frac{1}{2}(L_{ij} + L_{ji})$.

A.3. Some useful functions

The equation of the ellipse is given by:

$$\frac{x^2}{a^2}+\frac{y^2}{b^2}-1=0 \tag{25}$$

Define the function $\lambda(x,y)$ such that it is the positive root of:

$$\frac{x^2}{a^2+\lambda(x,y)}+\frac{y^2}{b^2+\lambda(x,y)}-1=0 \tag{26}$$

If $\lambda(x,y)$ is a constant then a family of elliptical curves is defined. Alternatively if we select any point (x,y) then there is a particular value of $\lambda(x,y)$ that can be calculated. For conciseness we denote $\lambda(x,y)$ simply as λ, but must remember that it is actually a function. Another function P of x and y is defined as:

$$\frac{1}{P^2}=\frac{x^2}{(a^2+\lambda)^2}+\frac{y^2}{(b^2+\lambda)^2} \tag{27}$$

Using implicit differentiation the following are derived:

$$\frac{\partial\lambda}{\partial x}=\frac{2P^2x}{a^2+\lambda} \tag{28}$$

$$\frac{\partial\lambda}{\partial y}=\frac{2P^2y}{b^2+\lambda} \tag{29}$$

If we define $\Delta(\lambda)$:

$$\Delta(\lambda)=\sqrt{(a^2+\lambda)(b^2+\lambda)} \tag{30}$$

If sometimes we use Δ then we mean $\Delta(\lambda)$, in all other cases we specify the argument explicitly. Then the following integrals are of interest (i.e. will appear as part of the solution):

$$\alpha=\int_\lambda^\infty\frac{\mathrm{d}\xi}{(a^2+\xi)\Delta(\xi)} \tag{31}$$

$$\beta=\int_\lambda^\infty\frac{\mathrm{d}\xi}{(b^2+\xi)\Delta(\xi)} \tag{32}$$

$$\gamma=\int_\lambda^\infty\frac{\mathrm{d}\xi}{(a^2+\xi)(b^2+\xi)\Delta(\xi)} \tag{33}$$

Jefferys (1922) did not use a different symbol under the integral, which may be confusing. Note also that ξ is a function of x and y. The 3D equivalent expressions have a closed form solution as given by Jezek et al. (1999) and we can evaluate the above to be (Mandal et al., 2001):

$$\alpha=\frac{2}{a^2-b^2}\left(1-\frac{b^2+\lambda}{\Delta}\right) \tag{34}$$

$$\beta=\frac{2}{a^2-b^2}\left(-1+\frac{a^2+\lambda}{\Delta}\right) \tag{35}$$

$$\gamma=\frac{2}{(a^2-b^2)^2}\left(-2+\frac{a^2+b^2+2\lambda}{\Delta}\right) \tag{36}$$

which are all functions of x and y due to the presence of λ. The symbols α_0, β_0, γ_0 and Δ_0 are defined as α, β, γ and Δ evaluated at $\lambda=0$.

In determining a solution to the problem we will assume a solution in terms of functions which are solutions to Laplace's equation. That is for some function $f(x,y)$ we have:

$$\nabla^2 f=\frac{\partial^2 f}{\partial x^2}+\frac{\partial^2 f}{\partial y^2}=0 \tag{37}$$

Our solution will be written in terms of the following two functions (and their derivatives):

$$\Omega(x,y)=\int_\lambda^\infty\left(\frac{x^2}{a^2+\xi}+\frac{y^2}{b^2+\xi}-1\right)\frac{\mathrm{d}\xi}{\Delta(\xi)} \tag{38}$$

$$\chi(x,y)=\gamma xy \tag{39}$$

By differentiating we find that:

$$\frac{\partial\Omega}{\partial x}=2x\alpha \tag{40}$$

$$\frac{\partial\Omega}{\partial y}=2y\beta \tag{41}$$

$$\frac{\partial^2\Omega}{\partial x^2}=2\alpha-\frac{4P^2x^2}{(a^2+\lambda)^2\Delta} \tag{42}$$

$$\frac{\partial^2\Omega}{\partial y^2}=2\beta-\frac{4P^2y^2}{(b^2+\lambda)^2\Delta} \tag{43}$$

$$\frac{\partial^2\Omega}{\partial x\partial y}=-\frac{4P^2xy}{(a^2+\lambda)(b^2+\lambda)\Delta} \tag{44}$$

and also that:

$$\frac{\partial\chi}{\partial x}=\gamma y-\frac{2P^2x^2y}{(a^2+\lambda)^2(b^2+\lambda)\Delta} \tag{45}$$

$$\frac{\partial\chi}{\partial y}=\gamma x-\frac{2P^2xy^2}{(a^2+\lambda)(b^2+\lambda)^2\Delta} \tag{46}$$

A.4. Assumed solution

First we note the following identities due to Ω being a solution to Laplace's equation:

$$x\frac{\partial^2\Omega}{\partial x^2}-\frac{\partial\Omega}{\partial x}=-x\frac{\partial^2\Omega}{\partial y^2}-\frac{\partial\Omega}{\partial x} \tag{47}$$

$$y\frac{\partial^2\Omega}{\partial y^2}-\frac{\partial\Omega}{\partial y}=-y\frac{\partial^2\Omega}{\partial x^2}-\frac{\partial\Omega}{\partial y} \tag{48}$$

Our assumed solution is written in terms of the above as:

$$u = u_0 + T\frac{\partial\chi}{\partial x} + W\frac{\partial\chi}{\partial y} + A\left(x\frac{\partial^2\Omega}{\partial x^2} - \frac{\partial\Omega}{\partial x}\right) + H\left(x\frac{\partial^2\Omega}{\partial x\partial y} - \frac{\partial\Omega}{\partial y}\right) + y\left(H'\frac{\partial^2\Omega}{\partial x^2} + B\frac{\partial^2\Omega}{\partial x\partial y}\right) \quad (49)$$

$$v = v_0 + T\frac{\partial\chi}{\partial y} - W\frac{\partial\chi}{\partial x} + B\left(y\frac{\partial^2\Omega}{\partial y^2} - \frac{\partial\Omega}{\partial y}\right) + H'\left(y\frac{\partial^2\Omega}{\partial x\partial y} - \frac{\partial\Omega}{\partial x}\right) + x\left(H\frac{\partial^2\Omega}{\partial y^2} + A\frac{\partial^2\Omega}{\partial x\partial y}\right) \quad (50)$$

Using these equations we can derive an expression for the pressure, p, which will be of use in determining the stress field. First of all, only terms multiplied by x or y in Eqs. (49) and (50) will be non-zero in $\nabla^2 u$ and $\nabla^2 v$ due to χ and Ω being solutions to Laplace's equation. Therefore:

$$\nabla^2 u = 2\left[B\frac{\partial^3\Omega}{\partial x\partial y^2} + (H + H')\frac{\partial^3\Omega}{\partial x^2\partial y} + A\frac{\partial^3\Omega}{\partial x^3}\right] \quad (51)$$

$$\nabla^2 v = 2\left[B\frac{\partial^3\Omega}{\partial y^3} + (H + H')\frac{\partial^3\Omega}{\partial x\partial y^2} + A\frac{\partial^3\Omega}{\partial x^2\partial y}\right] \quad (52)$$

which from Eqs. (22)–(24) implies that:

$$p = p_0 + 2\mu\left[B\frac{\partial^2\Omega}{\partial y^2} + (H + H')\frac{\partial^2\Omega}{\partial x\partial y} + A\frac{\partial^2\Omega}{\partial x^2}\right] \quad (53)$$

where p_0 is an arbitrary constant.

Next we substitute our expression for χ and Ω into Eqs. (49) and (50) (however, we first apply the identity in Eq. (47) to the coefficient of A in Eq. (49) and the identity in Eq. (48) to the coefficient of B in Eq. (50)) to get:

$$u = (L_{11} + \gamma W - 2A(\alpha + \beta))x + (L_{12} - 2\beta H + 2\alpha H' + \gamma T)y - \frac{2P^2 x}{\Delta(a^2+\lambda)}\left(\frac{(2H(a^2+\lambda) + 2H'(b^2+\lambda) + T)xy}{(a^2+\lambda)(b^2+\lambda)} + \frac{(2B(b^2+\lambda) - 2A(a^2+\lambda) + W)y^2}{(b^2+\lambda)^2}\right) \quad (54)$$

$$v = (L_{21} + 2\beta H - 2\alpha H' + \gamma T)x + (L_{22} - \gamma W - 2B(\alpha + \beta))y - \frac{2P^2 y}{\Delta(b^2+\lambda)}\left(\frac{(2A(a^2+\lambda) - 2B(b^2+\lambda) - W)x^2}{(a^2+\lambda)^2} + \frac{(T + 2H'(b^2+\lambda) + 2H(a^2+\lambda))xy}{(a^2+\lambda)(b^2+\lambda)}\right) \quad (55)$$

At this stage Jefferys made the assumption that the object was rigid and therefore could only rotate. From now on our solution differs to that of Jefferys (1922). We assume that the ellipse can both deform homogeneously and rotate and use subscript i for referring to this internal object flow. Hence we assume that the internal motion is:

$$u_i = kx + \omega_1 y \quad (56)$$

$$v_i = -\omega_2 x - ky \quad (57)$$

At the surface of the ellipse (i.e. $\lambda = 0$) the internal and external flows must agree. At $\lambda = 0$ we have:

$$u = (L_{11} + \gamma_0 W - 2A(\alpha_0 + \beta_0))x + (L_{12} - 2\beta_0 H + 2\alpha_0 H' + \gamma_0 T)y - \frac{2P^2 x}{\Delta a^2}\left(\frac{(2Ha^2 + 2H'b^2 + T)xy}{a^2 b^2} + \frac{(2Bb^2 - 2Aa^2 + W)y^2}{b^4}\right) \quad (58)$$

$$v = (L_{21} + 2\beta_0 H - 2\alpha_0 H' + \gamma_0 T)x + (L_{22} - \gamma_0 W - 2B(\alpha_0 + \beta_0))y - \frac{2P^2 y}{\Delta b^2} \times \left(\frac{(2Aa^2 - 2Bb^2 - W)x^2}{a^4} + \frac{(T + 2H'b^2 + 2Ha^2)xy}{a^2 b^2}\right) \quad (59)$$

By equating coefficients we derive the following relationships that must be satisfied:

$$\begin{aligned} L_{11} + \gamma_0 W - 2A(\alpha_0 + \beta_0) &= k \\ L_{12} - 2\beta_0 H + 2\alpha_0 H' + \gamma_0 T &= \omega_1 \\ 2Ha^2 + 2H'b^2 + T &= 0 \\ 2Bb^2 - 2Ab^2 + W &= 0 \\ L_{21} - 2\beta_0 H - 2\alpha_0 H' + \gamma_0 T &= -\omega_2 \\ L_{22} - \gamma_0 W - 2B(\alpha_0 + \beta_0) &= -k \end{aligned} \quad (60)$$

which on solution gives:

$$A = \frac{(\alpha_0 + \beta_0)(L_{11} - k) - b^2\gamma_0(L_{11} + L_{22})}{2(\alpha_0 + \beta_0)(\alpha_0 + \beta_0 - (a^2 + b^2)\gamma_0)}$$

$$B = \frac{(\alpha_0 + \beta_0)(L_{22} + k) - a^2\gamma_0(L_{11} + L_{22})}{2(\alpha_0 + \beta_0)(\alpha_0 + \beta_0 - (a^2 + b^2)\gamma_0)}$$

$$W = \frac{a^2(L_{11} - k) - b^2(L_{22} + k)}{\alpha_0 + \beta_0 - (a^2 + b^2)\gamma_0}$$

$$H = \frac{\alpha_0(L_{12} + L_{21} - \omega_1 + \omega_2) + b^2\gamma_0(L_{12} - L_{21} - \omega_1 - \omega_2)}{4(a^2\alpha_0 + b^2\beta_0)\gamma_0}$$

$$H' = \frac{\beta_0(L_{12} + L_{21} - \omega_1 + \omega_2) - a^2\gamma_0(L_{12} - L_{12} - \omega_1 - \omega_2)}{4(a^2\alpha_0 + b^2\beta_0)\gamma_0}$$

$$T = -\frac{L_{12} + L_{21} - \omega_1 + \omega_2}{\gamma_0} \quad (61)$$

A.5. Stress field

In order to derive the values of ω_1, ω_2 and k we must consider and equate the internal and external stress fields at the ellipse boundary. For the internal case the pressure is everywhere constant, p_{i0}. The internal stresses (denoted by superscript (i)) are therefore:

$$\begin{aligned} \sigma_{xx}^{(i)} &= 2\mu_i k - p_{i0} \\ \sigma_{yy}^{(i)} &= -2\mu_i k - p_{i0} \\ \sigma_{xy}^{(i)} &= \mu_i(\omega_1 - \omega_2) \end{aligned} \quad (62)$$

and the external stresses (denoted by superscript (e)) evaluated at the boundary (i.e. $\lambda=0$) are:

$$\sigma_{xx}^{(e)} = -p_{e0} + \mu_e \left[\begin{array}{c} \dfrac{2abk + (b^2-a^2)(k-L_{11})}{ab} \\ +P^2\left(\dfrac{2(3b^2(L_{12}-\omega_1)+a^2(L_{21}-\omega_2)+2ab(L_{12}+L_{21}-\omega_1+\omega_2))xy}{a^3b^3} - \dfrac{(a+b)^2(k-L_{11})x^2}{a^5b} + \dfrac{(a+b)^2(k-L_{11})y^2}{ab^5} \right) \\ -P^4\left(\dfrac{4(a+b)(b(L_{12}-\omega_1)+a(L_{21}+\omega_2))x^3y}{a^7b^3} + \dfrac{4(a+b)^2(k-L_{11})x^2y^2}{a^5b^5} \right) \end{array} \right]$$

$$\sigma_{yy}^{(e)} = -p_{e0} + \mu_e \left[\begin{array}{c} \dfrac{-2abk + (b^2-a^2)(k-L_{11})}{ab} \\ +P^2\left(\dfrac{2(b^2(L_{12}-\omega_1)+3a^2(L_{21}+\omega_2)+2ab(L_{12}+L_{21}-\omega_1+\omega_2))xy}{a^3b^3} - \dfrac{(a+b)^2(k-L_{11})x^2}{a^5b} + \dfrac{(a+b)^2(k-L_{11})y^2}{ab^5} \right) \\ -P^4\left(\dfrac{4(a+b)(b(L_{12}-\omega_1)+a(L_{21}+\omega_2))xy^3}{a^3b^7} - \dfrac{4(a+b)^2(k-L_{11})x^2y^2}{a^5b^5} \right) \end{array} \right]$$

$$\sigma_{xy}^{(e)} = \mu_e \left[\begin{array}{c} \omega_1-\omega_2 + P^2\left(\dfrac{2a(L_{21}+\omega_2)+b(L_{12}+L_{21}-\omega_1+\omega_2)x^2}{a^4b} + \dfrac{2b(L_{12}-\omega_1)+a(L_{12}+L_{21}-\omega_1+\omega_2)y^2}{a^4b} \right) \\ -P^4\left(\dfrac{4(a+b)(b(L_{12}-\omega_1)+a(L_{21}+\omega_2))x^2y^2}{a^5b^5} + \dfrac{2(a+b)^2(k-L_{11})xy^3}{a^3b^7} - \dfrac{2(a+b)^2(k-L_{11})x^3y}{a^7b^3} \right) \end{array} \right] \tag{63}$$

In order to equate the internal and external stresses at the boundary the unit normal vector (**n**) to the boundary of the ellipse is first calculated using the gradient (Marsden and Tromba, 2003, p. 170):

$$\mathbf{n} = P\begin{pmatrix} \dfrac{x}{a^2} \\ \dfrac{y}{b^2} \end{pmatrix} \tag{64}$$

The stress vector is calculated by multiplying the stress tensor by the unit normal (Lai et al., 1993, p. 173):

$$\mathbf{t} = P\begin{pmatrix} \sigma_{xx} & \sigma_{xy} \\ \sigma_{xy} & \sigma_{yy} \end{pmatrix} \bullet \begin{pmatrix} \dfrac{x}{a^2} \\ \dfrac{y}{b^2} \end{pmatrix} = P\begin{pmatrix} \dfrac{x\sigma_{xx}}{a^2} + \dfrac{y\sigma_{xy}}{b^2} \\ \dfrac{x\sigma_{xy}}{a^2} + \dfrac{y\sigma_{yy}}{b^2} \end{pmatrix} \tag{65}$$

If we denote the first component by X and the second component by Y then our internal and external stresses become:

$$\begin{aligned} \sigma_X^{(i)} &= P\left(\frac{(2\mu_i k - p_{i0})x}{a^2} + \frac{\mu_i(\omega_1-\omega_2)y}{b^2} \right) \\ \sigma_Y^{(i)} &= P\left(\frac{\mu_i(\omega_1-\omega_2)x}{a^2} - \frac{(2\mu_i k + p_{i0})y}{b^2} \right) \\ \sigma_X^{(e)} &= P\left(\frac{(2a\mu_e(L_{11}-k)+b(2L_{11}\mu_e - p_{e0}))x}{a^2b} \right. \\ &\qquad \left. + \frac{\mu_e(a(L_{12}+L_{21})+2b(L_{12}-\omega_1))y}{ab^2} \right) \\ \sigma_Y^{(e)} &= P\left(\frac{\mu_e(b(L_{12}+L_{21})+2a(L_{12}+\omega_2))x}{a^2b} \right. \\ &\qquad \left. - \frac{(2b\mu_e(L_{11}-k)+a(2L_{11}\mu_e + p_{e0}))y}{ab^2} \right) \end{aligned} \tag{66}$$

So by equating the x and y coefficients, the stress equality at the boundary is satisfied and the following solution is achieved

where it is arbitrarily assumed that $p_{i0}=0$ and letting $\mu_r=\mu_e/\mu_i$:

$$\begin{aligned} k &= \frac{\mu_r(a+b)^2 L_{11}}{\mu_r(a^2+b^2)+2ab} \\ \omega_1 &= \frac{2abL_{12}\mu_r + a^2(L_{12}\mu_r + L_{21}(\mu_r-1)) + b^2 L_{12}}{2ab\mu_r + a^2 + b^2} \\ \omega_2 &= -\frac{2abL_{12}\mu_r + b^2(L_{21}\mu_r + L_{12}(\mu_r-1)) + a^2 L_{21}}{2ab\mu_r + a^2 + b^2} \\ p_{e0} &= -\frac{2(a^2-b^2)L_{11}\mu_r(\mu_r-1)}{2ab+\mu_r(a^2+b^2)} \end{aligned} \tag{67}$$

Appendix B. Constructing a solution

From Eqs. (56) and (57) the internal motion is:

$$\frac{dx}{dt} = kx + \omega_1 y \qquad \frac{dy}{dt} = -\omega_2 x - ky \tag{68}$$

The general equation of an ellipse centred on the origin is:

$$Ax^2 + By^2 + Cxy - 1 = 0 \tag{69}$$

noting that all the coefficients and x and y depend on time. Differentiate Eq. (69) and substitute in Eq. (68) to get:

$$x^2\left(\frac{dA}{dt} + 2Ak - C\omega_2\right) + y^2\left(\frac{dB}{dt} - 2Bk + C\omega_1\right) + xy\left(\frac{dC}{dt} + 2A\omega_1 - 2B\omega_2\right) = 0 \tag{70}$$

which is satisfied by letting the coefficients be zero, giving expressions for dA/dt, dB/dt and dC/dt. Now the orientation of the long axis of a general ellipse is:

$$\phi = \frac{1}{2}\tan^{-1}\left(\frac{C}{A-B}\right) \tag{71}$$

Note that at the exact instant we are interested in $C=0$ (i.e. the ellipse is parallel to the x,y coordinate system), so that by differentiating both sides and substituting for dA/dt, dB/dt and dC/dt and letting $A=1/a^2$ and $B=1/b^2$:

$$\frac{d\phi}{dt} = \frac{b^2\omega_1 - a^2\omega_2}{a^2-b^2} \tag{72}$$

After substituting for ω_1, ω_2 and the flow field with respect to the fixed coordinate system:

$$\frac{d\phi}{dt} = \frac{1}{2}(L'_{21} - L'_{12}) + \frac{(a+b)(a^2+b^2+2ab(\mu_r-1))((L'_{12}+L'_{21})\cos 2\phi - 2L'_{11}\sin 2\phi)}{2(a-b)(a^2+b^2+2ab\mu_r)} \tag{73}$$

As a quick check, consider a rigid object (i.e. $\mu_r=0$) in simple shear flow (i.e. $L'_{12}=\dot{\gamma}$ and all other components zero) then:

$$\frac{d\phi}{dt} = -\dot{\gamma}\left(\frac{a^2\sin^2\phi + b^2\cos^2\phi}{a^2+b^2}\right) \tag{74}$$

which is equivalent to the expression of Ghosh and Ramberg (1976, Eq. 1) taking into account the slightly different definitions for ϕ (i.e. we take $\phi=0$ as the positive x-axis, whereas Ghosh and Ramberg take $\phi=0$ as the positive y-axis).

A similar analysis for the long and short axis lengths gives:

$$\frac{da}{dt} = ak \tag{75}$$

$$\frac{db}{dt} = -bk \tag{76}$$

and substituting for k and the flow field with respect to the fixed coordinate system:

$$\begin{aligned} \frac{da}{dt} &= \frac{a(a+b)^2\mu_r(2L'_{11}\cos 2\phi + (L'_{12}+L'_{21})\sin 2\phi)}{2((a^2+b^2)\mu_r + 2ab)} \\ \frac{db}{dt} &= -\frac{b(a+b)^2\mu_r(2L'_{11}\cos 2\phi + (L'_{12}+L'_{21})\sin 2\phi)}{2((a^2+b^2)\mu_r + 2ab)} \end{aligned} \tag{77}$$

References

Arbaret, L., Fernandez, A., Jezek, J., Ildefonse, B., Launeau, P., Diot, H., 2000. Analogue and numerical modeling of shape fabrics: application to strain and flow determination in magmas. Transactions of the Royal Society of Edinburgh: Earth Sciences 90, 97–109.

Bilby, B.A., Kolbuszewski, M.L., 1977. The finite deformation of an inhomogeneity in two-dimensional slow viscous incompressible flow. Proceedings of the Royal Society London, Series A 355, 335–353.

Bilby, B.A., Eshelby, J.D., Kundu, A.K., 1975. The change of shape of a viscous ellipsoidal region embedded in a slowly deforming matrix having a different viscosity. Tectonophysics 28, 265–274.

Chang Man Fong, C.F., De Kee, D., 1999. Perturbation Methods, Instability, Catastrophe and Chaos. World Scientific, New Jersey.

Coelho, S., Passchier, C.W., Grasemann, B., 2005. Geometric description of flanking structures. Journal of Structural Geology 27, 597–606.

Dunnet, D., 1969. A technique of finite strain analysis using elliptical particles. Tectonophysics 7, 117–136.

Eshelby, J.D., 1957. The determination of the elastic field of an ellipsoidal inclusion, and related problems. Proceedings of the Royal Society London, Series A 241, 376–396.

Exner, U., Mancktelow, N.S., Grasemann, B., 2004. Progressive development of s-type flanking folds in simple shear. Journal of Structural Geology 26, 2191–2201.

Fletcher, R.C., 1977. Folding of a single viscous layer: exact infinitesimal-amplitude solution. Tectonophysics 39, 593–606.

Fletcher, R.C., 2004. Anisotropic viscosity of a dispersion of aligned elliptical cylindrical clasts in viscous matrix. Journal of Structural Geology 26, 1977–1987.

Fry, N., 1979. Random point distributions and strain measurement in rocks. Tectonophysics 60, 806–807.

Gay, N.C., 1968. Pure shear and simple shear deformation of inhomogeneous viscous fluids. 1. Theory. Tectonophysics 5, 211–234.

Ghosh, S.K., 1987. Measure of non-coaxiality. Journal of Structural Geology 9, 111–113.

Ghosh, S.K., Ramberg, H., 1976. Reorientation of inclusions by combination of pure shear and simple shear. Tectonophysics 34, 1–70.

Grasemann, B., Stüwe, K., 2001. The development of flanking folds during simple shear and their use as kinematic indicators. Journal of Structural Geology 23, 715–724.

Grasemann, B., Stüwe, K., Vannay, J., 2003. Sense and non-sense of shear in flanking structures. Journal of Structural Geology 25, 19–34.

Jefferys, G.B., 1922. The motion of ellipsoidal particles immersed in a viscous fluid. Proceedings of the Royal Society of London A 102, 201–211.

Jezek, J., Hrouda, F., 2002a. Software for modeling the magnetic anisotropy of strained rocks. Computers and Geosciences 28, 1061–1068.

Jezek, J., Hrouda, F., 2002b. A technique for numerical modeling of magnetic anisotropy to strain relationship. Physics and Chemistry of the Earth 27, 1247–1252.

Jezek, J., Saic, S., Segeth, K., Schulmann, K., 1999. Three-dimensional hydrodynamical modelling of viscous flow around a rotating ellipsoidal inclusion. Computers and Geosciences 25, 547–558.

Johnson, A.M., Fletcher, R.C., 1994. Folding of Viscous Layers. Columbia University Press, New York.

Lai, W.M., Rubin, D., Krempl, E., 1993. Introduction to Continuum Mechanics, 3rd ed Butterworth Heinemann, Oxford.

Lamb, H., 1932. Hydrodynamics. Cambridge University Press, Cambridge.

Lisle, R.J., 1994. Paleostrain analysis. In: Hancock, P.L. (Ed.), Continental Deformation. Pergamon Press, pp. 28–42.

Mancktelow, N.S., 1991. The analysis of progressive deformation from an inscribed grid. Journal of Structural Geology 13, 859–864.

Mandal, N., Chakraborty, C., Samanta, S.K. 2001. Flattening in shear zones under constant volume: a theoretical evaluation. Journal of Structural Geology 23, 1771–1780.

Marsden, J.E., Tromba, A.J., 2003. Vector Calculus. W.H. Freeman and Company.

Middleton, G.V., Wilcock, P.R., 1994. Mechanics in the Earth and Environmental Sciences. Cambridge University Press, Cambridge.

Mulchrone, K.F., 2003. Application of Delaunay triangulation to the nearest neighbour method of strain analysis. Journal of Structural Geology 25, 689–702.

Mulchrone, K.F., Grogan, S., Prithwijit, De., 2005. The relationship between magmatic tiling, fluid flow and crystal fraction. Journal of Structural Geology 27, 179–197.

Mulchrone, K.F., O' Sullivan, F., Meere, P.A., 2003. Finite strain estimation using the mean radial length of elliptical objects with bootstrap confidence intervals. Journal of Structural Geology 25, 529–539.

Passchier, C.W., 2001. Flanking structures. Journal of Structural Geology 23, 951–962.

Passchier, C.W., Trouw, R.A.J., 1996. Microtectonics. Springer, Berlin.

Ramberg, H., 1975. Particle paths, displacement and progressive strain applicable to rocks. Tectonophysics 28, 1–37.

Ramsay, J.G., 1967. Folding and Fracturing of Rocks. McGraw-Hill, New York.

Ramsay, J.G., Huber, M.I., 1983. The Techniques of Modern Structural Geology. Volume 1: Strain Analysis. Academic Press, London.

Schmid, D.W., Podladchikov, Y.Y., 2003. Analytical solutions for deformable elliptical inclusions in general shear. Geophysical Journal International 155, 269–288.

Smith, R.B., 1975. Unified theory of the onset of folding, boudinage, and mullion structure. Geological Society of America Bulletin 86, 1601–1609.

Strogatz, S.H., 1994. Nonlinear Dynamics and Chaos with Applications to Physics, Biology, Chemistry, and Engineering. Perseus Books, Reading, Massachusetts.

Taylor, G.I., 1932. The viscosity of a fluid containing small drops of another fluid. Proceedings of the Royal Society (London) A138, 41–48.

Treagus, S.H., 2002. Modelling the bulk viscosity of two-phase mixtures in terms of clast shape. Journal of Structural Geology 24, 57–76.

Treagus, S.H., Treagus, J.E., 2001. Effects of object ellipticity on strain, and implications for clast–matrix rocks. Journal of Structural Geology 23, 601–608.

Treagus, S.H., Treagus, J.E., 2002. Studies of strain and rheology of conglomerates. Journal of Structural Geology 24, 1541–1567.

Wiesmayr, G., Grasemann, B., 2004. Sense and non-sense of shear in flanking structures with layer-parallel shortening: implications for fault-related folds. Journal of Structural Geology 27, 249–264.